Sintering, crystallization, and properties of a low-viscosity SnO–MgO–P$_2$O$_5$ glass

Jiin-Jyh Shyu · Chih-Hsien Yeh

Abstract A lead-free, low-viscosity SnO–MgO–P$_2$O$_5$ glass powder was fabricated. Sinterability, wetting, flowability, crystallization, and the resulting properties of the glass powder were investigated. It is shown that the powder compact can be fully densified above 362 °C and show good wet to the substrate above 417 °C. The properties (coefficient of thermal expansion and chemical durability) of the sintered glass depend on the sintering temperature and are discussed in terms of the development of crystalline phases during sintering.

Introduction

Sealing glasses are used for facilitating joining between different parts such as glasses, metals, and ceramics [1]. Conventional low-melting sealing glasses, e.g., PbO–B$_2$O$_3$–SiO$_2$, PbO–ZnO–B$_2$O$_3$, and PbO–ZnO–SiO$_2$, usually contain higher amounts of lead [2], and thus having serious problems from environmental viewpoint. Phosphate glasses, as a representative glass system of low viscosity, are potentially important in sealing applications of CRT envelope [3, 4], OLED device [5], electronics [6], and ceramics packing [7, 8]. The major disadvantages of phosphate glasses are that their chemical durability is usually poor [9–11] and that their coefficients of thermal expansion (CTE, 60–180 × 10^{-7} K^{-1} [12–14]) are too high to match several low-CTE materials such as silicon. Sn–P–O–F glasses with ultra-low glass transition temperatures (T_g), good chemical durability, and relatively high CTE (180–280 × 10^{-7} K^{-1}) have been reported [15, 16]. The T_g and glass softening temperature (T_s) of the SnO–P$_2$O$_5$ glasses increase linearly with increasing SnO content in the range of 40–60 mol% SnO [17]. The 67SnO–33P$_2$O$_5$ (mol%) glass with high transmission in the visible-to-IR region and high refractive index has also been reported [18]. Moreover, the SnO–P$_2$O$_5$ glasses also are used as anode materials for lithium secondary batteries [19]. Morena [4, 20], Yamanaka [21], and Taketami [22] reported that SnO–ZnO–P$_2$O$_5$ glass system has low softening temperature and is a possible alternative to the Pb-based seal glasses. Bismuth-based glasses have also been developed for low-temperature sealing [23–26], which have CTE values of 90–110 × 10^{-7} K^{-1}. We recently published a new glass system SnO–MgO–P$_2$O$_5$ (SMP) that has low softening temperatures and good chemical durability [27]. The glass formation and properties (glass transition temperature, coefficient of thermal expansion, and chemical durability) of the as-cast glasses have been investigated.

Sealing glasses are usually applied in powder form. Moreover, the properties of low-viscosity glasses after thermal treatment are expected to be different from those of the parent glass, resulted from the development of crystalline phases. Therefore, in the present article, the sinterability, wetting, flowability, crystallization, and the resulting properties of the glass powder with a nominal composition of 60SnO–10MgO–30P$_2$O$_5$ (mol%) were investigated.

J.-J. Shyu (✉) · C.-H. Yeh
Department of Materials Engineering, Tatung University, Taipei 104, Taiwan, ROC
e-mail: jjshyu@ttu.edu.tw

C.-H. Yeh
e-mail: d9307003@ms.ttu.edu.tw

Experimental procedures

Sample preparation

The glass with the nominal composition of 60SnO, 10MgO, and 30P_2O_5 (mol%) was prepared from reagent-grade $Sn_2P_2O_7$ and MgO. The MgO powder was obtained from calcining $Mg(OH)_2$ powder at 700 °C for 1 h. Well-mixed powder containing the above chemicals and 1 wt% of sugar was placed in an alumina crucible. The batch was put directly into a furnace at 950–1000 °C in a nitrogen atmosphere. Nitrogen atmosphere and sugar were able to provide a reducing atmosphere during melting to inhibit the oxidation of Sn^{2+} to Sn^{4+}. After heating for 15–25 min, the melt was quenched in deionized water to form glass frits. The dried frits were crushed in an alumina-lined mortar grinder (model RMO, F. Kurt Retsch GmbH & Co. KG, Haan, Germany), then were sieved to obtain a glass powder with particle sizes between 37 and 44 µm.

The glass powder was uniaxially pressed in a steel die to yield disc-shaped samples (diameter 5 mm and thickness 3.5 mm). The green compacts were placed on soda-lime-silicate glass substrates. The sintered bodies were formed by heating the system at a rate of 10 K/min to 362–485 °C and held for 10 min in air, then furnace cooled.

Characterization

The as-quenched glass was dissolved in 36% HCl for chemical analysis using inductively coupled plasma optical emission spectrometry (ICP-OES, model Optima 2000, Perkin Elmer, Connecticut, USA). Glass transition temperature and crystallization temperature of the glass powder were measured by differential thermal analysis (DTA, model SDT 2960, TA Instruments, New Castle, DE, USA) at a heating rate of 10 K/min. The softening point (viscosity $10^{7.65}$ poise) of the parent glass was measured using a softening point tester (model SP-3A, Edward Orton Jr., Westerville, Ohio, USA) which has been calibrated by using NIST standards. Phase identification of the sintered samples was conducted by powder X-ray diffraction (XRD) analysis. Measurements were performed on a diffractometer (Model M21X, MAC Science, Yokohamo, Japan) with CuK$_\alpha$ radiation. The operating power was 40 kV and 200 mA. A sampling time of 1 s for each interval of 0.02° (2θ) was used. The sintered samples were polished with the aid of water or oil, and then coated with a thin film of gold for scanning electron microscopy (SEM, model JSM-5600, Jeol, Tokyo, Japan) observations. The diameter of the contact area between the sintered sample and substrate was measured. To measure the contact angle between the sintered sample and substrate, the image of the sessile drop

after being cooled to the room temperature was recorded with a digital camera. The contact angle was measured from both sides of the sessile drop using an optical contact angle measuring instrument (model OCA20, DataPhysics Instruments GmbH, Filderstadt, Germany). For water durability test, the sintered samples were cut by ultrasonic cutter to yield disc-shaped samples (diameter 9.9 mm and thickness 2.1 mm). The samples were polished with No. 1200 SiC paper and then ultrasonically cleaned with acetone. The samples were placed in covered polypropylene flasks containing 100 mL of deionized water at 90 °C for 30–360 min. At least three samples were used for each sintering condition. Then, the average dissolution rate, defined as the weight loss per unit surface area per unit time, was calculated. The CTE (30–225 °C) of the sintered samples was measured by thermomechanical analysis (TMA, model Setsys-1750, Setaram Inc., France), using fused quartz as push rod. The heating rate was 10 K/min. At least seven samples were used for each sintering condition.

Results and discussion

Effects of melting temperature/time on the composition and thermal properties of the as-quenched glass

Chemical analyses of the as-quenched glasses show that the glass composition varies with the melting temperature/time and consists of 59.40–61.39 mol% SnO, 9.94–10.31 mol% MgO, 26.94–29.04 mol% P_2O_5, and 1.24–1.60 mol% Al_2O_3 which comes from the alumina crucibles. It was found in the present study that the glass properties depend mainly on the Al_2O_3 content. Figure 1 shows that the Al_2O_3 content
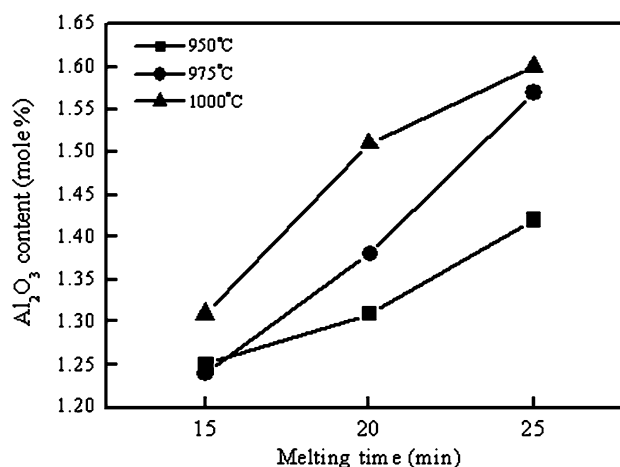
Fig. 1 Variation of Al_2O_3 content of the glasses melted at 950–1000 °C for 15–25 min
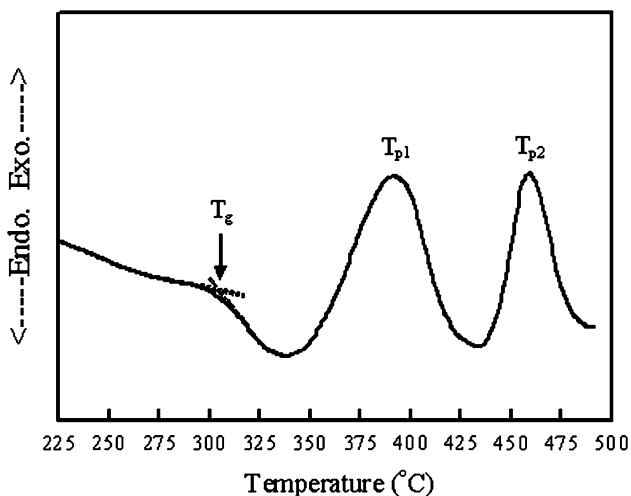
Fig. 2 DTA thermogram of the glass powder melted at 950 °C for 15 min

increases reasonably with the increasing melting temperature and melting time. Typical DTA thermogram of the glass powder is shown in Fig. 2. Glass transition temperature (T_g) and positions of the exothermic peaks due to glass crystallization (T_{P1} and T_{P2} for low- and high-temperature peaks, respectively) are indicated. Figure 3 shows that the values T_g, T_{P1}, and T_{P2} increase generally with the increasing melting temperature and time, possibly resulted from the increased glass viscosity due to the increased Al_2O_3 content. Because the glass powder obtained by melting at 950 °C for 15 min exhibits the lowest amount of Al_2O_3 (and thus the lowest T_g value), it was investigated in the following experiment. Moreover, the T_g values of the present glasses are in the range of 310–321 °C, being lower than those of PbO–ZnO–B_2O_3 (PZB) glass (about 328–335 °C [28]) and Bi_2O_3–B_2O_3-based glasses (about 325–500 °C [29–31]).
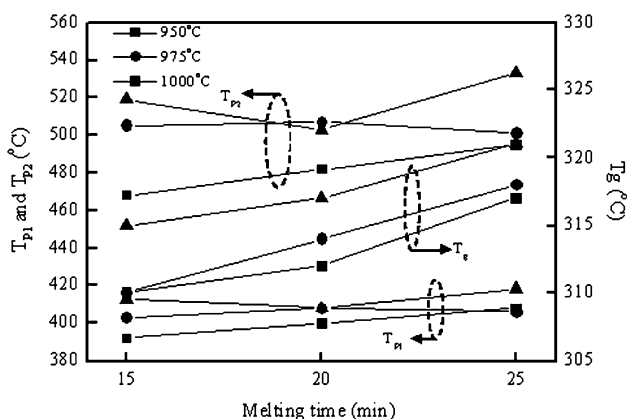
Crystalline phase formation and microstructure development of the heated glass

As shown in Fig. 2, the two exothermic peaks at 390 °C and 458 °C indicate that at least two crystalline phases have formed during heating. According to the XRD and SEM-EDS analyses (described in the next paragraph), the crystalline phases formed at low- and high temperature are $Mg_3(PO_4)_2$ (ICDD card no. 33-0876, denoted as M_3P) and $Sn_3(PO_4)_2$ (ICDD card no. 70-0391, denoted as S_3P), respectively.

Figures 4 and 5a–f show the typical XRD patterns and microstructures, respectively, of the samples sintered at 362–485 °C for 10 min. The softening point (viscosity $10^{7.65}$ poise) of the parent glass, measured by a penetration method, is 357 °C. The low softening point explains the fully densified microstructure at 362 °C, as shown in Fig. 5a. The XRD analysis indicated that those samples sintered at temperatures ≤377 °C were still amorphous. At 392 °C, crystalline particles (indicated by the arrow in Fig. 5b) with a diameter of about 2–3 μm began to form in the glass matrix. The corresponding XRD pattern in Fig. 4 did not reveal signals of diffraction lines, because that the amount of the crystalline phase is too low to be detected. This phase was identified as M_3P according to the XRD patterns of the samples sintered at higher temperatures (e.g., the 404 °C-pattern in Fig. 4) as well as the Mg- and P-rich compositions observed in the EDS analysis. $Mg_3(PO_4)_2$ crystals have also been found to form in the glass system SiO_2–P_2O_5–Al_2O_3–MgO–Na_2O [32]. It has been reported that only $Mg_2P_4O_{12}$ phase was formed during the crystallization of magnesium metaphosphate ($Mg(PO_4)_2$) glasses [33]. As seen in the 404 °C-pattern in Fig. 4, a S_3P phase also developed in addition to the major phase M_3P. The S_3P particles (indicated by the dotted arrow in Fig. 5c–d) show an elongated

Fig. 3 Variations of glass transition temperature (T_g) and DTA exothermic peak temperatures (T_{P1} and T_{P2}) of the glasses melted at 950–1000 °C for 15–25 min
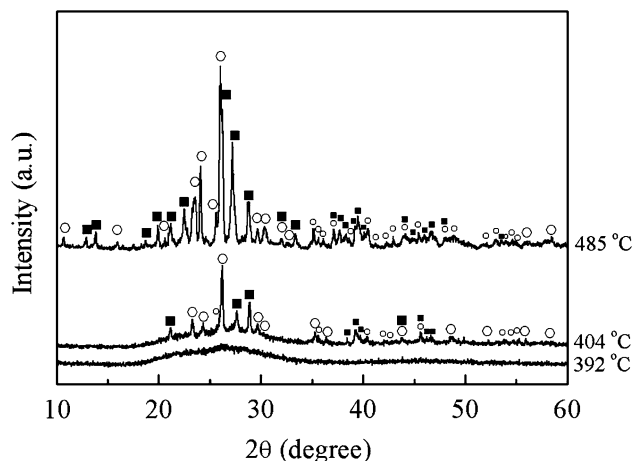
Fig. 4 Typical XRD patterns of the samples sintered at 392–485 °C for 10 min. The parent glass was melted at 950 °C for 15 min. (○ $Mg_3(PO_4)_2$ and ■ $Sn_3(PO_4)_2$)

Fig. 5 SEM micrographs of the samples sintered at **a** 362 °C, **b** 392 °C, **c–d** 404 °C, and **e–f** 485 °C for 10 min. The samples were polished with the aid of **a–e** oil and **f** water. The parent glass was melted at 950 °C for 15 min
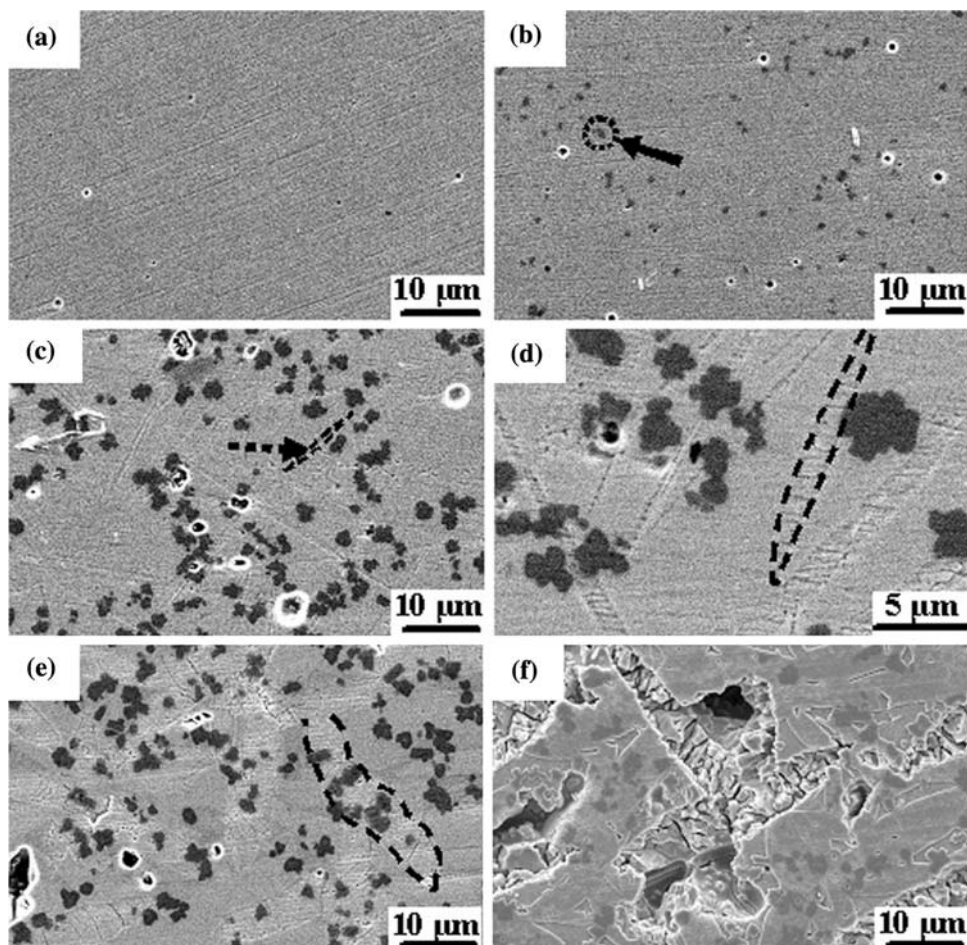
shape with an Sn- and P-rich composition confirmed by the EDX analysis. When the sintering temperature was further increased to 485 °C (Figs. 4 and 5e), the amounts of both the crystalline phases were still increased. Comparing the EDS result of the 485 °C-sample with that of the parent glass, the residual glass at 485 °C is nearly Mg-free, indicating that almost all the Mg ions have reacted with P to form the M_3P phase at this temperature. The microstructures shown in Fig. 5a–e were prepared by polishing the samples with the aid of oil. Figure 5f shows the microstructure of the 485 °C-sample polished with the aid of water. Comparing Fig. 5e with Fig. 5f indicates that the S_3P phase was much more easily attacked by water than the M_3P phase and even the residual glass matrix.

Flowability and wetting

Figure 6 shows the appearance, contact angle, and flow diameter (defined as the diameter of the contact area between sample and substrate) of the samples sintered at 362–485 °C for 10 min. The curves in Fig. 6 can be
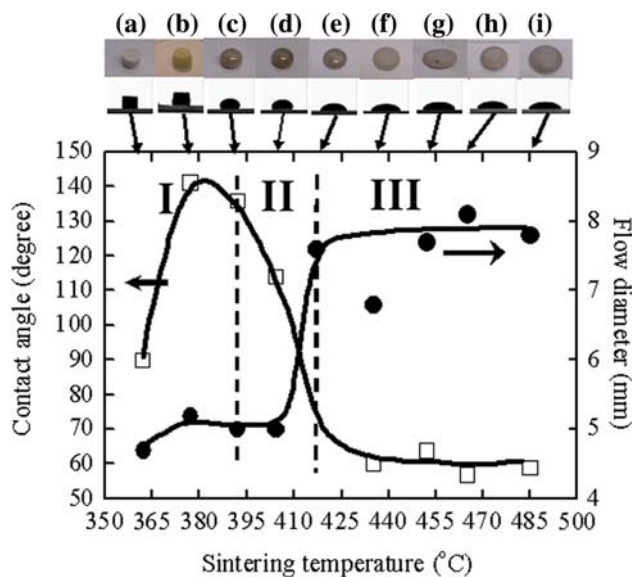
Fig. 6 Appearance, contact angle, and flow diameter of the samples sintered at **a** 362 °C, **b** 377 °C, **c** 392 °C, **d** 404 °C, **e** 417 °C, **f** 435 °C, **g** 452 °C, **h** 465 °C, and **i** 485 °C for 10 min. The parent glass was melted at 950 °C for 15 min

divided into three stages. Sintering temperature ≤392 °C is the stage I. Although the softening point (viscosity $10^{7.65}$ poise) of the parent glass is 357 °C, the contour of the sample was not changed at 362 °C (Fig. 6a). The contour of the sample became round with the increasing temperature (Fig. 6b–c). The contact angle is increased from 90° to about 135–141° due to gravitational force. The flow diameter at 362 °C is smaller than 5 mm due to densification. When sintering temperature is from 362 to 404 °C, the flow diameter was only slightly increased because the glass viscosity is still high. The stage II is characterized by a significant drop in contact angle (135° to around 60°) and remarkable increase in flow diameter in a very narrow temperature range (392–417 °C). In stage III (sintering temperature ≥417 °C), both of the contact angle (about 60°) and flow diameter remained nearly constant, possibly because that the remarkable crystallization inhibited further softening and spreading of the glass. Moreover, the glass crystallization also changed the appearance of the sample surface from glossy (Fig. 6c–e) to mat (Fig. 6f–i).

Chemical durability and thermal expansion coefficient of the heated glass

Figure 7a and b shows the weight loss per unit area of the cast glass and the samples sintered at 362–377 °C for 10 min immersed in 90 °C deionized water for 30–360 min. The cast glass and the samples sintered at temperatures ≤404 °C exhibited a linear variation of weight loss with time (Fig. 7a). However, the samples sintered at temperatures ≥417 °C showed a nonlinear relationship (Fig. 7b). The rate of weight loss decreased when the immersion time was prolonged. The values of average dissolution rate, DR, were calculated from the weight-loss data. Figure 8 shows the variation of DR for immersion times of 1, 2, and 6 h with the sintering temperature. Those samples sintered at 362–392 °C showed dissolution rates close to that of the cast glass. The dissolution rate began to decrease at 392 °C and reached a minimum at 404–417 °C, possibly due to the development of M_3P phase. When the sintering temperature was further increased, the dissolution rate began to increase due to the formation of S_3P phase that is more easily attacked by water than M_3P and the residual glass matrix. The decreased dissolution rate with prolonged immersion time, as shown in Fig. 7b, can be explained by that the fraction of the S_3P phase on the sample surface was reduced with the immersion time. The data for a commercialized PZB glass are also shown in Fig. 7a and b for comparison. It is shown that the chemical durability of the samples sintered at 404–465 °C is superior to the PZB glass. Because of the poor chemical durability of the S_3P phase, further work is in progress to suppress the development of this phase.
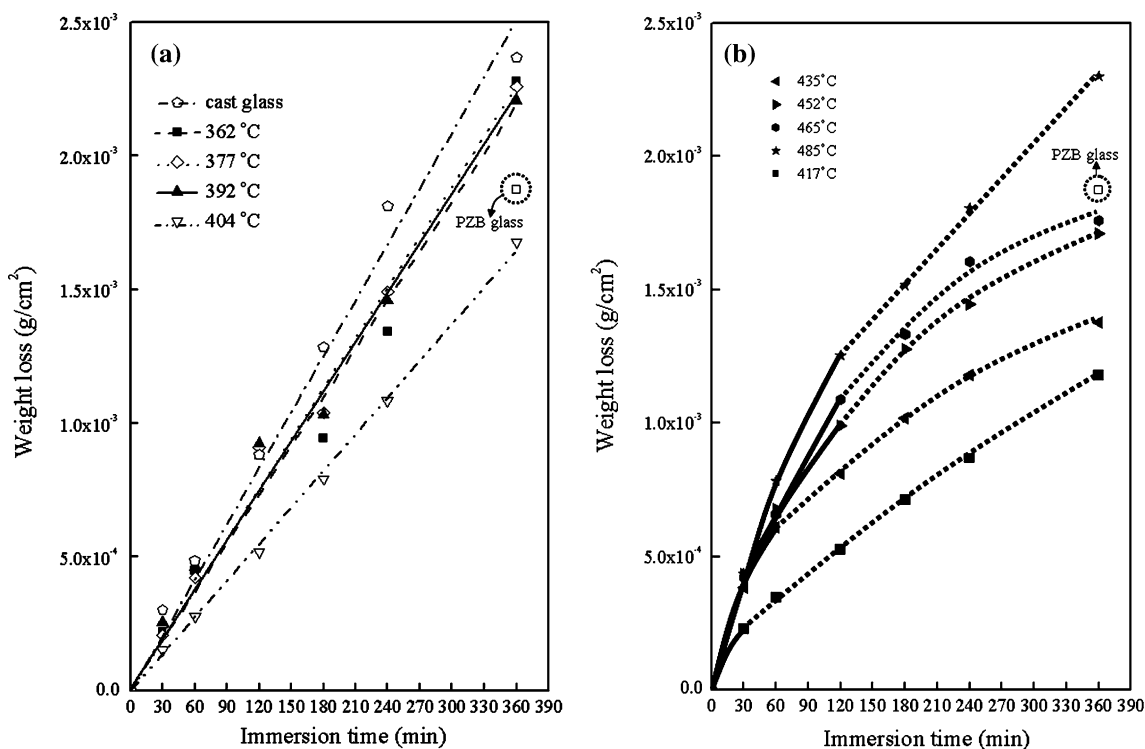
Fig. 7 Variation of the weight loss per unit area in 90 °C water with the immersion time for **a** cast glass and the samples sintered at 362–404 °C, and **b** the samples sintered at 417–485 °C. The parent glass was melted at 950 °C for 15 min. The data for a commercialized PbO–ZnO–B$_2$O$_3$ (PZB) glass are also shown for comparison
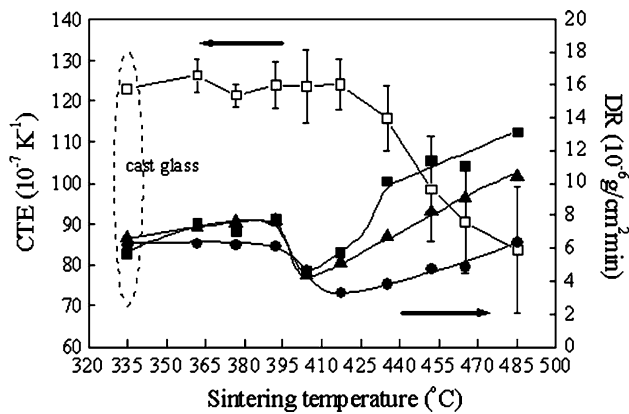
Fig. 8 Variations of coefficient of thermal expansion and average dissolution rate (immersion time = 1 h (■), 2 h (▲), and 6 h (●)) with sintering temperature of the samples sintered at 362–485 °C for 10 min. The parent glass was melted at 950 °C for 15 min

The variation of CTE of the samples with sintering temperature is also shown in Fig. 8. The CTE values of the samples sintered below 417 °C were nearly unchanged with respect to the cast glass (CTE = 123×10^{-7} K^{-1}). This result implies that that the CTE value of M$_3$P phase might be close to that of the glass phase. The CTE values of the samples decreased with the sintering temperature when the sintering temperature was higher than 410 °C. This trend might imply that the S$_3$P phase has a CTE value smaller than the parent glass. The CTE value was reduced to 84×10^{-7} K^{-1} when the sintering temperature was increased to 485 °C. The CTE values of SnO–P$_2$O$_5$-based glasses are reported to be about 100–140 [17, 22] and 180–280 $\times 10^{-7}$ K^{-1} [15, 16] for glass compositions without and with F$^-$, respectively. The CTE values of PZB glass and Bi$_2$O$_3$–B$_2$O$_3$-based glasses are reported to be about 65–120 [1, 28] and 105–122 $\times 10^{-7}$ K^{-1} [29–31], respectively.

Conclusions

(1) Melting of the SnO–MgO–P$_2$O$_5$ glass in alumina crucible resulted in the contamination of Al$_2$O$_3$ and thus increased both the glass transition temperature and crystallization temperature.

(2) The SnO–MgO–P$_2$O$_5$ powdered glass can be fully densified above 362 °C and is obviously softened above 392 °C. The softened glass shows the optimum spreading on substrate above 417 °C.

(3) The glass powder can be devitrified after sintering. The first crystalline phase, Mg$_3$(PO$_4$)$_2$, begins to form at around 392 °C. The crystalline phase formed at higher temperatures (≥404 °C) is Sn$_3$(PO$_4$)$_2$.

(4) The material properties (coefficient of thermal expansion and chemical durability) of the glass are changed after sintering and are mainly determined by the crystalline phases developed.

(5) As compared with the parent glass, the development of Mg$_3$(PO$_4$)$_2$ crystals in the sintered material improves the chemical durability while almost does not affect the CTE. The development of Sn$_3$(PO$_4$)$_2$ crystals is harmful to the chemical durability, although it is able to reduce CTE.

(6) The CTE value of the sintered material is in the range of 84–123 $\times 10^{-7}$ K^{-1} and generally decreases with the increase in sintering temperature. Optimum chemical durability of the sintered material is reached in an intermediate range of sintering temperature (404–417 °C).

References

1. Takamori T (1979) In: Momozawa M, Doremus RH (eds) Treatise on materials science and technology, vol 17. Academic Press, p 177
2. Takamori T (1979) In: Momozawa M, Doremus RH (eds) Treatise on materials science and technology, vol 17, Academic Press, p 247
3. Morena R (1996) USP 5,516,733
4. Morena R (1996) USP 5,514,629
5. Aitken BG, An CP, Quesada MA (2007) USP 2007/0252526
6. Shell JA, Ohio T (1976) USP 3,970,464
7. Krüger R, Roosen A, Schaper W (1999) J Eur Ceram Soc 19:1067
8. Guonel MJ-F, Norton MG (2004) J Non-Cryst Solids 347:173
9. Brow RK (2000) J Non-Cryst Solids 263 & 264:1
10. Takebe H, Baba Y, Kuwabara M (2006) J Non-Cryst Solids 352:3088
11. Bunker BC, Arnold GW, Wilder JA (1984) J Non-Cryst Solids 64:291
12. Brow RK, Tallant DR (1997) J Non-Cryst Solids 222:396
13. Karabulut M, Melini E, Stefan R, Mrasinghe GK, Ray CS, Kurkjian CR, Day DE (2001) J Non-Cryst Solids 288:8
14. Möncke D, Ehrt D, Velli LL, Varsamis CPE, Kamitsos EI (2005) Phys Chem Glasses 46:67
15. Xu XJ, Day DE (1990) Phys Chem Glasses 31:183
16. Tick PA (1983) USP 4,379,070
17. Popova E, Dimitriev Y (2007) J Mater Sci 42:3358. doi:10.1007/s10853-006-0787-z
18. Takebe H, Nonaka W, Kubo T, Cha J, Kuwabara M (2007) J Phys Chem Solids 68:983
19. Hayashi A, Konishi T, Tadanaga K, Minami T, Tatsumisago M (2004) J Non-Cryst Solids 345–346:478
20. Morena R (2000) J Non-Cryst Solids 263–264:382
21. Yamanka T (2003) USP 6,617,269
22. Taketami K (2003) JP 2003/252648
23. Hayakawa N, Shimooka T (2003) USP 2003/0228471
24. Usul H, Manabe T, Harada K, Tanbe R (1998) USP 5,733,828
25. Yuzo K, Tatauya K (2002) JP 2002/241143
26. Hiroshi U, Tsuneo M, Kazuo H, Ryuichi T (1998) JP 10139478

27. Shyu JJ, Yeh CH (2007) J Mater Sci 42:4772. doi:10.1007/s10853-006-0766-4
28. Robert A (1983) USP 4,478,947
29. Noriaki M (2006) JP 2006282501
30. Saritha D, Markandeya Y, Salagram M, Vithal M, Singh AK, Bhikshamaiah G (2008) J Non-Cryst Solids 354:5573
31. Bale S, Rahmana S, Awasthi AM, Sathe V (2008) J Alloys Compd 460:699
32. Aboud T, Stoch L (1997) J Non-Cryst Solids 219:149
33. Saltzberg MA, Hu YH (1990) J Am Ceram Soc 73:2970